Characteristics of the H-Mode Pedestal and Extrapolation to ITER

T.H. Osborne,[1] J.G. Cordey,[2] R.J. Groebner,[1] T. Hatae,[3] A. Hubbard,[4] L.D. Horton,[5] Y. Kamada,[3] A. Kritz,[6] L.L. Lao,[1] A.W. Leonard,[1] A. Loarte,[7] M.A. Mahdavi,[1] D. Mossessian,[4] T. Onjun,[6] M. Ossenpenko,[8] T.D. Rognlien,[9] G. Saibene,[7] P.B. Snyder,[1] M. Sugihara,[10] R. Shurygin,[8] K. Thomsen,[7] M.R. Wade,[11] H.R. Wilson,[2] X.Q. Xu,[9] K. Yatsu,[12] and the International Tokamak Physics Activity H-Mode Pedestal Working Group

[1]General Atomics, P.O. Box 85608, San Diego, California 92186-5608
e-mail: osborne@fusion.gat.com
[2]EURATOM/UKAEA Fusion Association, Culham Science Center, Abingdon, United Kingdom.
[3]Japan Atomic Energy Research Institute, Naka-machi, Ibaraki-ken, 311-0193 Japan.
[4]Massachusetts Institute of Technology, Cambridge, Massachusetts USA.
[5]Max Planck Institut für Plasmaphysik, 85748 Garching, Germany.
[6]Lehigh University, Bethlehem, Pennsylvania USA.
[7]EFDA-JET, Culham, United Kingdom.
[8]Institute of Nuclear Fusion, Kurchatov Institute, Russia.
[9]Lawrence Livermore National Laboratory, Livermore, California, USA.
[10]ITER Joint Work Site, Naka, Japan.
[11]Oak Ridge National Laboratory, Oak Ridge, Tennessee, USA.
[12]Plasma Research Center, University of Tsukuba, Tsukuba, Ibaraki 305-8577, Japan.

Abstract. The peeling-ballooning mode model for edge stability along with a model for the H-mode transport barrier width is used as an approach to estimating the H-mode pedestal conditions in ITER. Scalings of the barrier width based on ion-orbit loss, neutral penetration, and turbulence suppression are examined and empirical scalings of the barrier width are presented. An empirical scaling for the pedestal β is derived based on ideas from stability and the empirical width scaling. The impact of the stability model and other factors on ELM size is discussed.

1. Introduction

Although the H-mode transport barrier usually occupies less than 5% of the minor radius, the characteristics of this region have a strong impact on the expected performance of an H-mode based reactor. Stiff temperature profile, turbulent transport models [1,2] predict core temperatures, and hence energy confinement and fusion power production efficiency, to be highly dependent on the value of the temperature at the top of the H-mode pedestal. In order to meet the design goals of ITER these models require a minimum H-mode pedestal temperature of about 4 keV [3,4]. The high particle confinement also associated with H-mode leads to accumulation of core impurities unless some additional mode activity occurs in the region of the edge particle source. In standard H-mode the periodic ELM instability, which is triggered by the high pressure gradients obtainable in the H-mode transport barrier, controls the particle accumulation. However the very short duration of the ELM instability may result in unacceptable divertor heat loads.

This paper discusses progress in these areas through inter-machine comparison under the venue of the H-mode Pedestal Working Group of the International Tokamak Physics Activity (ITPA).

2. Edge Stability

It has become clear that the ideal, infinite *n*, ballooning mode first proposed as the ELM instability [5] does not set the edge pressure gradient limit. On DIII-D for example, the edge is in the second stable regime for infinite n ballooning with pressure gradients a factor of 2-3 above where the first stable limit would be, and the strong increase in edge pressure gradient observed with increasing triangularity is not consistent with infinite n ballooning mode predictions [6]. High triangularity, high elongation, and low aspect ratio increase the effect of geodesic curvature and reduce the normal curvature drive such that access to the second stable regime for infinite n ballooning modes is available even at moderately high shear. The bootstrap current associated with the edge pressure gradient reduces the magnetic shear which also improves access to the second stable regime. In addition, the high $k_\perp$ at high toroidal mode number is expected to result in finite Larmor radius stabilization above $n = 30$ [7]. Although high *n* pressure driven modes may be stabilized, lower n

modes can be triggered at higher pressure gradient. At lower *n*, resonant surfaces become more widely separated increasing the radial extent of the mode. This increases the effect of magnetic shear which both increases the critical pressure gradient, and reduces the value of the shear below which second stable access is obtained. The larger radial width of lower *n* modes also leads to a stabilizing effect when the radial mode width is larger than the extent of the steep pressure gradient region that provides the drive. This leads to a reduction in the pressure gradient limit at large transport barrier width which tends to reduce the variation in pedestal pressure with transport barrier width [7]. The large bootstrap currents expected to be associated with the high pressure gradient in the pedestal can in addition trigger current driven peeling modes [8]. The peeling and ballooning mode branches merge below some *n* value [9] blocking further access to higher pressure gradient regardless of the shear value. The inverse relation between shear and current density leads to a composite peeling-ballooning mode stability boundary in p', j_ϕ space shown qualitatively in Fig. 1(b). The GATO [10], MISHKA [11], and ELITE [12], codes have been used to compute peeling-ballooning mode stability for a number of tokamaks [13,14] with agreement between the code predictions and the pressure gradient limit before a Type I ELM. The peeling-ballooning mode model accounts for the high edge pressure gradients, the variation of gradient with shape [Fig. 1(a)], and the variation of the gradient with transport barrier width in DIII-D [7]. This model may also have an important consequence in terms of ELM size which will be discussed in Section 5. An ELITE prediction of the peeling ballooning mode model for the H-mode pedestal temperature in ITER is shown in Fig. 1(c). The model equilibria used in these calculations included a number of simplifications in the equilibrium construction process, including up-down symmetry (while matching the given separatrix elongation and triangularity), and lack of true X-points. In the pedestal region, the parallel current was taken to be equal to the bootstrap current, as calculated using the Sauter collisional model [15]. Estimates of the pedestal temperature set by the ITER requirement of Q=10 at P_{FUSION} = 400 MW depend on which turbulent transport model is used [3]. Recent results [16] give $T^{PED} \sim$ 4 keV from GLF23 and $T^{PED} \sim$ 2.5 keV for the less stiff Multimode model. These would give requirements for the pedestal width of $\Delta/a \sim$ 2.5% and $\Delta/a \sim$ 1% respectively, where this is the fraction of minor radius on the outboard midplane. Preliminary work [14] indicates that diamagnetic effects would raise the predicted pressure gradient limit for ITER significantly.

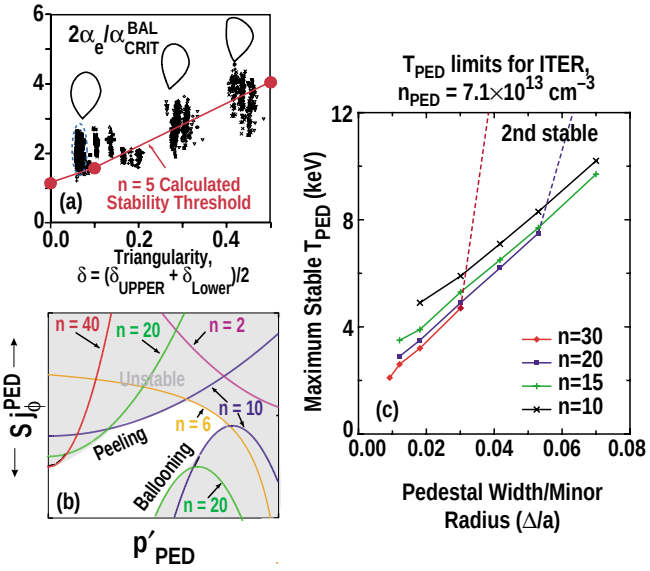

Fig. 1. (a) Peeling-ballooning stability calculation matches the variation in edge pressure gradient with triangularity in DIII-D, (b) schematic of peeling-ballooning stability contours, (c) stability calculation for ITER. Achieving T_{ped} = 4 keV requires an H-mode barrier width of 0.025 a.

3. H-Mode Transport Barrier Width

There is wide experimental and theoretical support for the flow shear turbulence suppression model of transport barrier formation in tokamaks [17]. Although turbulent transport models have made great progress in describing core transport, most have difficulty with the high magnetic shear and complex flux surface geometry of the region near the separatrix, and a full theoretical treatment of the H-mode transport barrier is not yet available. In this section we discuss three physics based arguments as to what might set the transport barrier width and examine how well they fit the available data and what they might predict for ITER.

The databases used in the present analysis are available to the international community through the ITPA. PDB3V2 includes pedestal information for Alcator C-Mod, ASDEX-Upgrade, DIII-D, JET,

and JT-60U, including both electron and ion pedestal parameters; however the data is generally averaged over ELMs although some ELM free data is available. D3DPED is comprised entirely of DIII-D data with Thomson scattering measurements of the electron pedestal parameters taken roughly every 10 ms in 173 discharges. The databases also hold MHD equilibrium parameters, ballooning mode stability analysis, ELM type indicators, and information giving the timing of each pedestal profile measurement relative to an ELM. It is important to note that edge stability and the limited variation of pedestal parameters over an ELM cycle introduce strong correlations into these databases. It is therefore essential that any empirical scaling law for the transport barrier width be shown to apply to both the ELM-free or inter-ELM periods as well as to the variation with different discharge conditions. At present there are transport barrier width measurements available for JT-60U, DIII-D, and Alcator C-Mod. For JT-60U the transport barrier width is taken to be the distance between the position of the knee at the top of the ion temperature pedestal and the separatrix, where the ion temperature profile is obtained from charge exchange recombination measurements, and the separatrix location is determined from equilibrium reconstruction based on magnetic measurements. In cases where electron temperature profile data is available from Thomson scattering for JT-60U, the barrier width inferred from this profile agrees with the ion measurements. For DIII-D and Alcator C-Mod the transport barrier width is derived from the electron temperature profiles from Thomson scattering measurements. Here the profiles are fit to a hyperbolic tangent form and the width is taken as the width of the steep gradient region independent of the equilibrium reconstruction. In DIII-D when CXR ion profiles are also available, the knee in the ion temperature profile is found to agree with that of the electrons, however the ion temperature gradient scale length is generally much longer than the electron and the ion temperature at the separatrix can be several hundred eV.

Some authors have suggested a scaling for the transport barrier width based on the process which might create the velocity shear. Shaing [18] and others have argued that the velocity shear which suppresses turbulence in the H-mode pedestal is driven by the $j\times B$ force associated with currents which must flow in response to the loss of ions on orbits that cross the separatrix. The range of this force is then roughly the width of the banana orbit for a barely trapped ion

$$\Delta \approx 2\, f_T\, \nu_{TOT}/\Omega_{Pi} \approx 2\sqrt{2\varepsilon/(1+\varepsilon)3T_i/m_i}\,\Big/\left(eB_P/m_i\right) = 2\sqrt{6\varepsilon/(1+\varepsilon)}\,\rho_{Pi} \quad . \tag{1}$$

where $\rho_{Pi}=\sqrt{T_i/m_i}\,/\Omega_{Pi}$. The radial electric field acts to squeeze the orbits giving [19] $\Delta\propto\rho_{Pi}/\sqrt{Q}$, where $Q=\left|1-E_r'/B_p\Omega_{Pi}\right|$. Since the ∇p term typically dominates the E_r determined from radial force balance $Q=1+\left(\rho_{Pi}/\Delta\right)^2$. Itoh [20] noted that viscosity would drive the shear flow region inward from the region where the force was present giving a scaling for the transport barrier width, $\Delta\propto\sqrt{\rho_{Pi}^2+\mu/\nu_i}$. The measured barrier width for the three machines is compared to Eq. (1) in Fig. 2 using averaged values for the poloidal field and radius (or width), $B_p=\sqrt{2\mu_0\left[(2/3)W/V\right]}/\beta_p$, $a_v=\sqrt{V/2\pi^2R}$, where W and V are the total stored energy and volume. Previous work on JT-60U [21] gave $\Delta_{Ti} \approx 2.3\rho_{Pi}$ for ELM-free discharges, where this relation held well over a range of safety-factor, $2 < q < 7$, and to some extent was independent of plasma shape over the range, $0.05 < \delta < 0.4$, $1.4 < \kappa < 1.7$. This is close to the value predicted by Eq. (1) for JT-60U, $\Delta = 2.2\ \rho_{Pi}$, or $\Delta = 2.0\ \rho_{Pi}$, with orbit squeezing. More recent JT-60U data for ELMing discharges, much at higher triangularity, departs from this scaling but a strong correlation with ρ_P is still clear. The DIII-D data lie near the predicted value however there is no clear trend with ρ_{Pi}. The

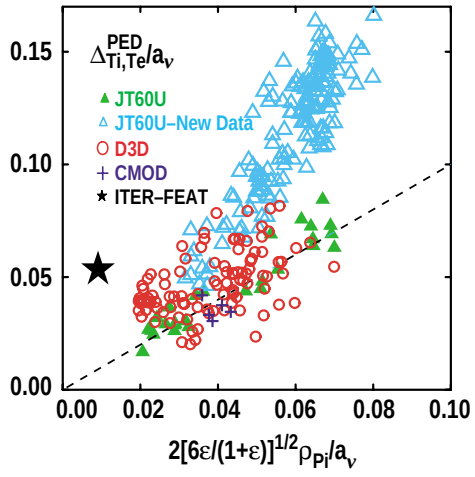

Fig. 2. Normalized transport barrier width shows some agreement with banana width. JT-60U data shows scaling with ρ_{pol}.

C-Mod data is also near the predicted value, and other data from C-Mod shows no correlation with ρ_{Pi} [22]. This scaling would give a pedestal width in ITER of $\Delta/a = 0.004$ ($\Delta_v/a_v \approx 0.01$) which would give an expected pedestal temperature of 1 keV for ITER based on the stability calculations of Fig. 1(c). [Note that the required value for ITER based on GLF23 from Fig. 1(c) is mapped from the midplane value to a_v in Fig. 2]. Experiments on DIII-D, however, in which divertor pumping and gas puffing were used to vary the pedestal temperature over a wide range indicated that a simple function of temperature could not account for both the variation of the width between ELMs and the overall behavior as the density was varied [23]. The JT-60U discharges are in a low collisionality regime where the viscosity term may be expected to play a role and result in a different scaling. In addition, DIII-D discharges where the ∇B drift direction was reversed did not show a significant change in transport barrier width although a significant change in orbit loss would be expected. These results suggest that a more detailed study of the possibility that the ion orbit loss region sets the transport barrier width is needed before it can be applied with confidence to a prediction for ITER.

In another approach to H-mode transport barrier width scaling, the process which creates E_r is not directly considered, rather it is assumed that any E_r profile consistent with the radial force balance can be obtained by adjusting the particle and power fluxes. Taking transport coefficients that were reduced continuously with increasing $E\times B$ velocity shear, Hinton and Staebler [24] demonstrated a transport bifurcation and derived a barrier width scaling set primarily by the edge localized neutral particle source

$$\Delta \approx \left[2\lambda L_n^{Sep} \ln\left(c\Gamma_{Sep} Q_{Sep}\right)\right]^{1/2} \quad , \tag{2}$$

where λ is the neutral mean free path, $\lambda = v_n/n_e \langle \sigma v \rangle$, L_n^{Sep} is the density gradient scale length at the separatrix, and Γ_{Sep}, Q_{Sep} are the particle and heat fluxes at the separatrix on which the width depends only logarithmically. Work on DIII-D [25] has shown that the shape of the density profile in the transport barrier is consistent with what would be expected for neutral penetration. In this model, when the density is sufficiently high, neutrals cannot cross the SOL to reach the main plasma without undergoing charge exchange or ionization (in which case they are recycled to the divertor). Thus, at high density, neutrals crossing the separatrix have acquired the velocity of the ions in this region $v_n \approx \sqrt{2T_i^{Sep}/\pi m_i}$. This type of process generally characterizes the DIII-D discharges. At low density, neutrals at the Frank-Condon velocity can cross the separatrix and reach regions of higher ion temperature. Since the charge exchange rate is actually somewhat larger than the ionization rate, a large fraction of the Frank-Condon neutrals can acquire velocities more characteristic of the H-mode pedestal temperature. This effect is further enhanced by the fact that above 300 eV the ionization rate decreases while the charge exchange rate continues to increase. The JT-60U discharges in the ITPA database with large widths are generally in the Frank-Condon dominated regime. Figure 3 shows a comparison between this neutral penetration model [25] and transport barrier widths. The C-Mod results are not included in the figure since almost dropoff all the density profile is predicted to be outside the separatrix making it difficult to relate the density profile to the particle source inside the separatrix. In this analysis the separatrix ion temperature for DIII-D is taken to be the temperature at 95% of the poloidal flux which may account for some of the large predicted values. Because of the high densities required in ITER for a high level of fusion

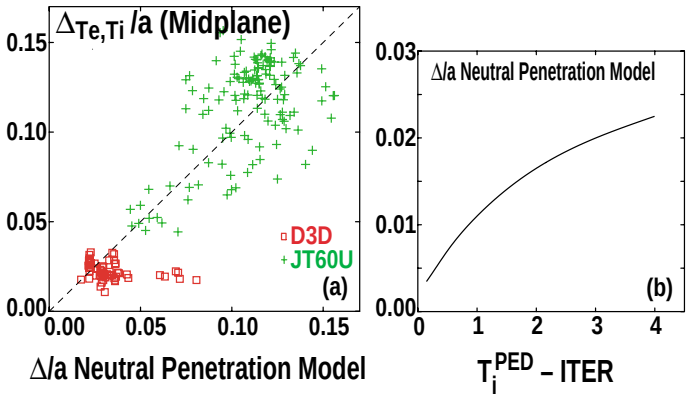

Fig. 3. (a) Comparison of transport barrier width on midplane and width of density steep gradient region inside the separatrix from neutral penetration. (b) Transport barrier width prediction for ITER as a function of separatrix ion temperature; the 3% width required by stability is only at very high T_i^{PED}

power, the ITER case is similar to DIII-D. A prediction of the ITER pedestal width based on this model as a function of separatrix ion temperature is shown in Fig. 3(b). This model suggests that, at least in the case of gas puff fueling, it would be difficult to obtain a large enough width based on stability considerations [Fig. 1(c)] unless the separatrix temperature was so high that it would be in conflict with the ITER divertor requirements.

Another approach to determining the barrier width is based on the idea the inner edge of the barrier is defined by the point at which the velocity shear is sufficient to quench the turbulence [26]. There is computational and theoretical support for the principle that the turbulence is quenched when the velocity shearing rate in the absence of turbulence exceeds the linear growth rate of the instabilities [26]. ITG modes still may dominate the region near the inner boundary of the transport barrier and we take as a guide the results from core transport simulations [26,27]. Typically the pressure gradient term dominates the radial electric field derived from ion radial force balance so that

$$\omega_{E\times B} \sim \frac{c_s^2}{\Delta^2 \Omega_{ci}} > \gamma_L \sim \frac{c_s}{a}\left(\frac{a}{\Delta}\right)^{\zeta_1}\left(\frac{T_e}{T_i}\right)^{\zeta_2} \Big/ \left[f(S,\alpha) g\left(Z_{eff}\right) h\left(\nu_{*s}\right)\right] \quad . \qquad (3)$$

The destabilizing effect of the temperature gradient is given by a/Δ taking the temperature gradient scale length as the transport barrier width. The coefficient ζ_1 is a function of type of instability, e.g. slab versus toroidal ITG; for shifted circles GLF23 simulations give $\zeta_1 \approx 3/2$ [27]. The T_e/T_i term is the stabilizing effect of high ion relative to electron temperature, for shifted circles $\zeta_2 \approx 3/2$ [27]. $f(S, \alpha)$ is a function that has a similar form to the $S, -\alpha$ diagram of the ideal MHD ballooning mode reflecting the similar effects of curvature and shear on ITG modes [27]. As with ideal MHD, at high magnetic shear increasing shear is stabilizing and increasing pressure gradient is destabilizing, while the opposite is true at low shear where something like a second stable regime occurs. We would perhaps expect this term to be a function of plasma shape as is case for ideal MHD. The term $g(Z_{eff})$ represents the stabilizing effect at high Z_{eff}. The term $h(\nu_{*s})$ represents the stabilizing effect of collisionality where the collision frequency in this case is normalized to the sound transit time characteristic of the eddy turnover time. For DIII-D, JT-60U, and ITER, $\nu_{*s} << 1$. Recent work [28] has shown that the effectiveness of the velocity shear is expected to be reduced at high elongation through essentially replacing the field in Ω_{ci} by $B_{EFF} \approx B_T \kappa$. Solving Eq. (3) for $\Delta_* = \Delta/a$ gives

$$\Delta_*^{1/2} = \rho_{*s}\left(\frac{T_i}{T_e}\right)^{1/2} f(S,\alpha) g\left(Z_{eff}\right) h\left(\nu_{*s}\right) \quad . \qquad (4)$$

The normalized width, Δ_*, is plotted against $\rho_{*s} = c_s/\Omega_{ci}$ for data from JT-60U, DIII-D and C-Mod in Fig. 4. It is clear that this quantity does not organize the data well; the small trend between DIII-D and JT-60U is coming mostly from the κ term in the effective field. Adding the temperature ratio term only further increases the scatter in such a plot. It should be noted that the scale length for the variation of the shear, and also possibly of the temperature ratio, and Z_{eff}, may be comparable to the transport barrier width which introduces an implicit dependence of the terms on the right hand side of Eq. (4) on Δ_*. For example, strong shear dependence could make the width more a function of the shear profile and only weakly dependent on ρ_{*s}. These considerations indicate that a more complete theoretical understanding of the behavior of the ITG growth rates in the pedestal region in real geometry is required before this type of argument can be applied to a prediction of the barrier width.

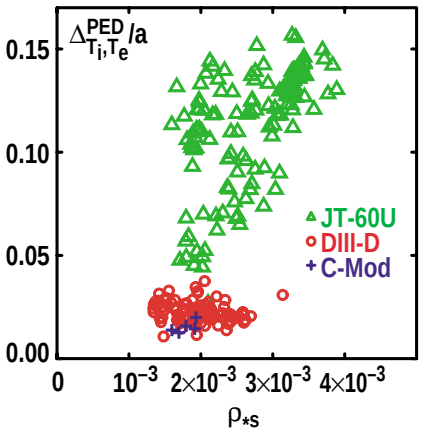

Fig. 4. Normalized transport barrier width on outer midplane is not well correlated with normalized gyroradius suggesting the more complex terms in Eq. (3) may be important.

Finally we consider an empirical scaling approach guided to some extent by the discussion above. The rather clear dependence of the JT-60U data on ρ_P suggests this type of term should be included. The

DIII-D data however suggests a mixture of density and temperature dependence. Previous empirical scaling work on DIII-D gave $\Delta_{pe} \propto \left(\beta_P^{PED}\right)^{0.4}$. As proposed by Hatae [29] we take a generalized scaling that allows for both effects by adding a dimensionally correct form for the density normalized to the Greenwald density $n_{*G} = 0.1\, n\, (10^{20}/\mathrm{m}^3)\, a^{1.75}/\mathrm{I_P}\ (\mathrm{MA})$. Since the average poloidal field is used in the JT-60U scaling this is also adopted. We also allow shape terms to account for their effect in the velocity shear and ITG growth rates. We fit to both a dimensionless and a form that allows for explicit size dependence. For the DIII-D we use the larger D3PED data set for ELM-free times only. This gives the best chance of setting the density and temperature terms independently. This results in the following scaling shown in Fig. 5. The size dependent fit gives

$$\Delta_* = 0.12 \pm 0.02 \times \rho_{*s}^{0.39\pm0.01} \left(B_T / B_P^{Ave}\right)^{0.31\pm0.01} n_{*G}^{0.19\pm0.01} \kappa^{-0.5\pm0.1} (1+\delta)^{0.57\pm0.04} R^{1.6\pm0.1} a^{-0.5\pm0.1} \quad . \qquad (5)$$

which is somewhat consistent with the behavior across the machines. This form predicts a pedestal width for ITER well above the value required by stability. Fitting to a dimensionless expression gives

$$\Delta_* = 0.044 \pm 0.006 \times \rho_{*s}^{0.38\pm0.01} \left(B_T / B_P^{Ave}\right)^{0.27\pm0.01} n_{*G}^{0.19\pm0.01} \kappa^{-0.98\pm0.04} (1+\delta)^{0.52\pm0.06} \varepsilon^{-2.3\pm0.1} \quad . \qquad (6)$$

which does not organize the different machines well. This fit still predicts the required pedestal width for ITER is also approximately met. The error bars given reflect only the uncertainties derived from the statistics of the fit but give some idea of the relative uncertainty of the different coefficients. Overall there is an unavoidable difference in the scaling between JT-60U which shows a temperature dependence but little density dependence, and DIII-D which shows more of a pressure dependence of the barrier width. We have so far not been able to resolve this difference to give good scaling in the individual machines and also between machines and the above expressions at most represent a compromise between the DIII-D and JT-60U dependencies.

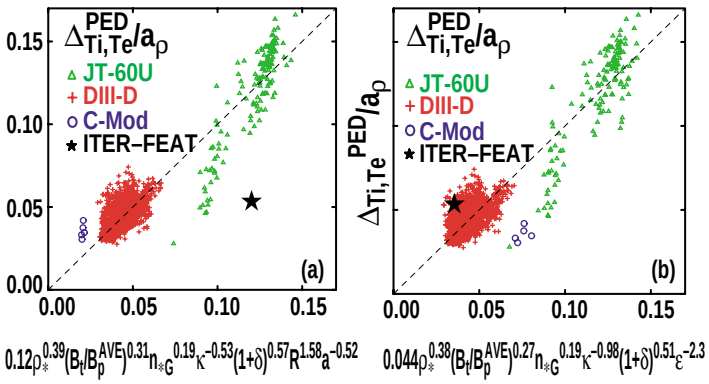

Fig. 5. Empirical fit of transport barrier width (a) fit to form including size dependence is more consistent with behavior between machines and predicts a very wide pedestal for ITER, (b) fit in dimensionless quantities does not match variation between machines as well.

4. H–Mode Pedestal Pressure Scaling

The dimensionless form of the empirical scaling for the transport barrier width, Δ_*, given in Eq. (6) can be applied to derive a scaling for the normalized pedestal pressure, β^{PED}, by assuming that the edge pressure gradient follows a ballooning mode scaling but with coefficients fit to account for strong shape dependence of peeling-ballooning modes. Experiments on DIII-D showed that the edge pressure gradient roughly followed ballooning scaling for a fixed shape. This suggests the relation $\beta^{PED}/\Delta_* = \varepsilon q^{-2}\, \alpha\,(\varepsilon,\kappa,\delta,S)$. The magnetic shear, S, is a strong function of the edge current density and therefore also the edge collisionality through its effect on the bootstrap current, and also of q and the plasma shape. Measurements of S are not currently available so we assume that this dependency can be absorbed into the shape and q dependencies and adopt a form $\beta^{PED}/\Delta_* = f\,(\varepsilon,\kappa,\delta,S)$. Fitting this to the full database gives Fig. 6. The derived scaling clearly does not match the individual machines adequately although it does give some order to

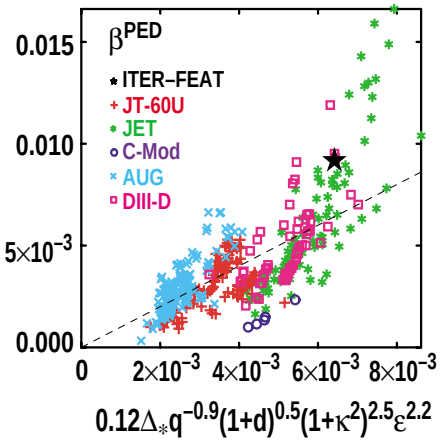

Fig. 6. Fit of pedestal toroidal beta using dimensionless width from Eq. (6). Individual machine trends are not well represented.

the variation between machines. The C-Mod points might be expected to be low since these are all either ELM-free or EDA-H-mode. The C-Mod points are low primarily as a result of the widths being poorly accounted for in Eq. (6) [Fig. 5(b)],

5. ELM Energy Loss

The power loads on the divertor plates that result from Type I ELMs can be of significant concern for a reactor scale tokamak. ELMs can result in a loss of as much as 20% of the energy in the H-mode pedestal W_{PED} = 3/2 P_{PED} V, where V is the total plasma volume, (Fig. 7) on a time scale of less than one millisecond [30–33]. To avoid significant erosion of the ITER divertor plates the ELM energy to the divertor must be kept below about 1 MJ/m^2 [34]. For the larger pedestals required by the GLF23 model for ITER, the pedestal energy is about 100 MJ. This means that the ELM energy loss must be less than about 5% of W_{PED}. Increasing the divertor area by tilting the target plates may raise this value to about 10% [35]. ELM energy loss data from several machines scales with edge collisionality (Fig. 7) which would predict unacceptably large ELMs for ITER ≈20%. On DIII-D, $\Delta W_{ELM}/W_{PED}$ is inversely correlated with n_e^{PED}/n_{GW} over a range of plasma shape and other discharge parameters [30. The DIII-D scaling would give $\Delta W_{ELM}/W_{PED} \approx 8\%$ for ITER. On DIII-D the toroidal mode number at the ELM onset increases as the ELM energy loss decreases at high density. This is consistent with ELITE code calculations showing that the most unstable n increases as the edge current density decreases with increased collisionality. The width of the linear eigenmode decreases as the transport barrier width and ELM energy loss decrease at high density. Other examples of a correlation between reduced eigenmode width and reduced ELM size include the grassy ELM regime on JT-60U [36], and the Type II ELM regime on ASDEX-Upgrade [37]. The width of the eigenmode generally tends to conform to the width of the steep gradient region. Since ITER requires roughly the same fractional pedestal width as existing machines this connection is of concern. However there is also evidence that the dependence of energy loss on barrier width can be broken. On DIII-D at high density the transport barrier width can be expanded while still maintaining small ELMs. Also, Thomson scattering measurements do not show much change in the extent of the ELM affected region as the ELM energy loss decreases with increased density on DIII-D [31]. Another concern is that the scaling relations for $\Delta W_{ELM}/W_{PED}$ represent only the average ELM while ELM energy loss in a discharge can be highly variable. Since the divertor effects represent a threshold condition even a small number of large ELMs could be a problem.

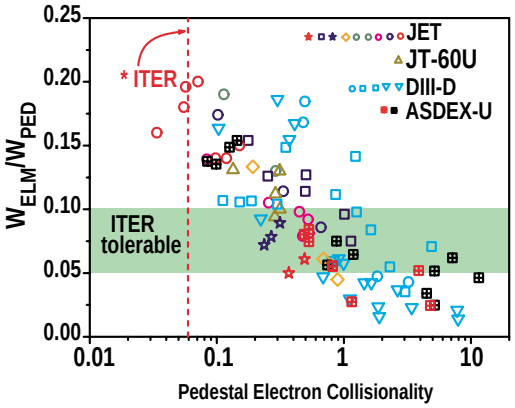

Fig. 7. ELM energy loss relative to pedestal energy decreases with increasing collisionality.

6. Conclusions

There remains large uncertainty in the prediction of both the ITER pedestal temperature and ELM energy loss. The peeling-ballooning model appears to fit the variation of the edge pressure gradient with shape and other parameters. It should be possible in the near future to verify this model quantitatively using a Lithium beam polarimetry diagnostic to measure edge current density on DIII-D. Understanding of the H-mode transport barrier width scaling is still far from complete. Although there is some correlation between poloidal gyroradius and the transport barrier width, there is also data in conflict with the idea that the loss region sets the barrier width. A more realistic calculation of the orbit loss region using an orbit following code should be carried out to verify this correlation. Even if orbit loss were the mechanism for shear flow generation, there is still significant work required to understand how the return current would be distributed and how the plasma rotation would respond. The neutral penetration picture also has some features consistent with the experiments, but needs to be

verified in more detail with 2-D particle transport codes. There is continuing progress in ITG/ETG mode calculations and it is hoped that in the near future these can be extended to the H-mode pedestal region in realistic geometry. At the present time it is difficult to apply ideas from ITG stability to the edge due to uncertainty in the possibly strong magnetic shear, collisionality, Z_{eff}, and temperature ratio effects. At least it can be said that, when one includes the improved edge stability coming from increased triangularity, ITER requires a transport barrier that is no larger a fraction of the minor radius than is common on existing machines. Also there is evidence from JT-60U that under some conditions this fraction increases with machine size. Current experiments typically have ELM energy loss that exceeds the acceptable values for the ITER divertor. However there are several regimes of reduced ELM energy such as the high density regime on DIII-D, the Type II ELM regime on AUG, and the grassy ELM regime at high triangularity on JT-60U. The EDA-H-mode and QH-mode [38] regimes in which the ELMs are replaced by continuous edge fluctuations offer the possibility of avoiding ELMs entirely.

Acknowledgment

This work was supported by the U.S. Department of Energy under Contracts DE-AC03-99ER54473, DE-FG02-92ER53214, W-7405-ENG-48, and DE-AC05-00OR22725. T.H. Osborne thanks F.W. Perkins, K.H. Burrell, G.M. Staebler, and J.E Kinsey for useful discussions.

References

[1] M. Kotscenreuter, *et al.*, in Proc. of 16th IAEA Conf., Montreal, (1996), IAEA-F1-CN-64/D1-5.
[2] R.E. Waltz, *ibid*, IAEA-F1-CN-64/D1-6.
[3] J.E. Kinsey, *et al.*, Proce. of the 24th Euro. Physical Society Conf., Berchtesgarten, III 1081 (1997).
[4] J.E. Kinsey, *et al.*, Burning Plasma Workshop II, May 2001.
[5] P. Gohil, *et al.*, Phys. Rev. Lett. **61**, 1603 (1998).
[6] T.H. Osborne, *et al.*, Plasma Phys. Control. Fusion **42**, A175 (2000) .
[7] J.R. Ferron, *et al.*, Phys. Plasmas **7**, 1976 (2000).
[8] J.W. Connor, *et al.*, Phys. Plasmas **5**, 2687 (1998).
[9] H.R. Wilson, *et al.*, Phys. Plasmas **6**, 1925 (1999).
[10] L.C. Bernard, *et al.*, Comp. Phys. Commun. **24**, 377 (1981).
[11] A.B. Mikailovskii, *et al.*, Plasma Phys. Rep. **23**, 844 (1997).
[12] H.R. Wilson, et al., Phys. Plasmas **9**, 1277 (2002).
[13] P.B. Snyder, *et al.*, Phys. Plasmas **9**, 2037 (2002).
[14] P.B. Snyder, this conference TH/3-1.
[15] O. Sauter, *et al.*, Phys. Plasmas **6** 2834 (1999).
[16] J.E. Kinsey, *et al.*, this conference TH/P1-09.
[17] K.H. Burrell, Phys. Plasmas **4**, 1499 (1997).
[18] K.C. Shaing, E.C. Scrume, Jr., Phys. Rev. Lett. **63**, 2369 (1989).
[19] K.C. Shaing, Phys. Fluids B **4**, 290 (1992).
[20] S.I. Itoh, *et al.*, Phys. Rev. Lett. **72**, 1200 (1994).
[21] T. Hatae, *et al.*, Plasma Phys. Control. Fusion **40**, 1073 (1998).
[22] J.W. Hughes, Phys Plasmas **9**, 3019 (2002).
[23] R.J. Groebner and T.H. Oborne, Phys. Plasmas **5**, 1800 (1998).
[24] F.L. Hinton, G.M. Staebler, Phys. Fluids B **5**, 1281 (1993).
[25] R.J. Groebner, *et al.*, Phys. Plasmas **9**, 2134 (2002).
[26] M. Kotschenreuther, et al., in Proc. of 16th IAEA Conf., Montreal (1996), F1-CN-64/D1-5.
[27] R.E. Waltz, *et al.*, Phys. Plasmas **4**, 2482 (1997).
[28] J.E. Kinsey, G.M. Staebler, and R.E. Waltz, Phys. Plasmas **9**, 1676 (2002).
[29] T. Hatae, *et al.*, Plasma Phys. Control. Fusion **42**, A283 (2000).
[30] A.W. Leonard, *et al.*, J. Nucl. Mater. **290-293**, 1097 (2001).
[31] A.W. Leonard, *et al.*, this conference.
[32] A. Loarte, *et al.*, this conference EX/P1-08.
[33] A. Asakura, *et al.*, this conference CT/P-01.
[34] G. Federici, *et al.*, in Proc. 15th Int. Conf. on Plasma Surface Interactions, PSI 2002.
[35] G. Federici, *et al.*, in Proc. 15th Int. Conf. on Plasma Surface Interactions, PSI 2002.
[36] L.L. Lao, *et al.*, Nucl. Fusion, **41**, 295 (2001).
[37] L.D. Horton, in Proc. of 29th Euro Physical Society Conf on Plasma Physics and Cont. Fusion, Montreux (2002).
[38] E.J. Doyle, *et al.*, this conference EX/C3-2.